Spring 2019

Age-Related Changes to Bone Microarchitecture in a Non-weight Bearing Bone

Tyler Hicks
tsh54@zips.uakron.edu

Janna M. Andronowski
jandronowski@uakron.edu

Reed Davis
rad11@zips.uakron.edu

Abstract

This study explored the relationship between age, sex and bone microarchitecture. Using high-resolution images, we may better understand the factors affecting different aspects of bone microstructure. Statistical support was provided for the quantitative differences in bone microarchitecture between the sexes. The significant differences noted in Canal Volume (Ca.V), Cortical Porosity (Ca.V/TV), Canal Surface (Ca.S) and Canal Surface to Tissue Volume (Ca.S/TV) offer several interesting points when compared with pre-existing literature. All four parameters listed above that reported significance did so with respect to sex, in that each parameter differed between sexes. However, no significant difference was noted among age within either sex. The biggest problem regarding the efficacy of this study was the small sample size for each age group. For any given age group, the sample size was not larger than 2 for each sex. This made it difficult to determine the effects of age on bone microstructure within one sex quantitatively. This may be due to the large of variation in the parameters we tested for. Support for age-related changes in bone microarchitecture within one sex, and additional support for changes between sex may be provided in the future when using a larger sample size.

Introduction

Identifying the age-at-death from bone tissue is critical in the analysis of unknown human remains. The standard macroscopic age estimation approach, which focuses on the evaluation and scoring of gross skeletal features, often suffices but can prove insufficient when skeletal remains are highly fragmented or commingled. In these scenarios, histological techniques are often applied. Evaluating rib bone microstructure could be key to overcoming this identification hurdle faced in the field of forensic anthropology. Studies have shown that exercise affecting the development of weight-bearing bone architecture does not affect the structure of non-weight bearing bone, specifically rib (Tommerup et al. 1993). This is a strong indicator for using rib samples, as it appears to be influenced less biomechanically by factors such as physical activity. Additionally, similar muscles are used among humans during respiration, with the diaphragm/intercostal muscles performing most frequently, and accessory muscles such as the obliques being used when respiration is forced (Taylor 1960). Although structures such as callus formation due to stress fractures can occur through actions such as repetitive rowing or chronic cough (Karlson 1998), rib bone remodeling due to muscle activity is largely limited by respiration; this is done so in a similar manner between individuals (Agnew and Stout 2012) and therefore argues that ribs are less vulnerable to variation from physical activity.

It is documented that bone remodeling occurs more rapidly in weight-bearing bone of females than males (Bell et al. 2001; Seeman 2013), and that ribs exhibit higher remodeling rates compared to weight-bearing bones (Epker and Frost 1965; Frost

1969). Osteon size in ribs is shown to have a detrimental affect on osteoblast/osteoclast activity, and therefore bone remodeling (Dominguez and Stout 2016). However, there is ambiguity as to whether sex is a determining factor of such remodeling in non-weight bearing bones (Dominguez and Stout 2016.)

There is much more support for age affecting bone loss and structural properties of bone (Epker and Frost 1965, Parfitt 1984, Agnew et al. 2015). Bone remodeling occurs on the largest scale during growth, where more bone is deposited than is resorbed (Seeman 2013). However, as one ages and bone remodeling continues, the result is a negative net bone loss in both cortical and trabecular bone; this can lead to larger resorptive spaces and increased fracture risk, especially in weight-bearing bones of postmenopausal women (Seeman 2013). Bone loss can be attributed to increased osteoclast activity, in which trabecular bone is removed, with cortical bone eventually meeting the same fate (Parfitt 1984). It is thought that the osteoclasts remove more bone, and penetrate deeper with age, while osteoblasts deposit thinner and thinner layers, ultimately causing net bone loss as individuals age (Parfitt 1984). Relating this to non-weight bearing bone such as rib, there is support that ribs would also show net bone loss with increased age. Not only is it well-documented that females exhibit greater bone loss, particularly after menopause (Dominguez and Stout 2016, Bell et al. 2001, Seeman 2013), but it has been shown that ribs show a higher bone remodeling rate overall (Epker and Frost 1965), and there is copious support for increasing age effecting the remodeling processes - a common denominator for age-related bone loss (Seeman 2013, Parfitt 1984, Agnew et al. 2015).

Methods for estimation age-at-death through forensic anthropological analysis has undergone development for decades, yet most popular methods are estimations still victimized by the huge variation due to the complicated processes of aging and the inherently complex microarchitecture. Researchers have known for quite some time that the microscopic structure of bone is different between age groups (Kerley 1965). However, these methods rely on quantifying osteons and canals found in bone, which are subject to large error rates (Ritz-Timme et al. 2000; Crowder 2005). Newer methods involved radiography such as taking MRIs of bone to determine age at the macroscopic level based on bone mineral density and bone volume (Hillewig et al. 2011), but some studies fail to find a sample size representative of the many ages at which a human can die - e.g. decedents under 30 years old. On a larger scale, failure to use ubiquitous statistical approaches or failure to note how drastic any error is in estimation may have contributed to the relative inability to accurately estimate age from bone (Ritz-Timme et al. 2000). The primary objectives of this study are to:1) explore changes in cortical and cancellous bone microstructure at the sixth-rib site across age categories and among the sexes, and 2) quantify cortical porosity and trabecular connectivity and other parameters to evaluate microstructural variation. By analyzing the microstructure of a non-weight bearing bone such as rib, a stronger connection between age and bone properties may be identified. It is hypothesized that several quantitative parameters being measured including bone volume, tissue volume, trabecular thickness and bone surface area will decrease as age increases, and will also be lower in females compared to males. Additionally, it is hypothesized that trabecular separation and

overall number of objects (cortical pores) will increase as age increases and will be higher in females compared to males.

Materials and Methods

SAMPLE PROCURMENT

Samples for this study were obtained through cadaver labs from medical schools cooperating with our lab, namely Northeastern Ohio Medical University (NEOMED), The University of Toledo College of Medicine and Life Science, and Kent State University. Specimens obtained from cadavers at these locations were collected within a time period of roughly one year (Dec.2017 - Dec. 2018). The sampling process occurred as follows: cleared the excision site of soft tissue, sawed near the midshaft with an oscillating saw to free a section of the left sixth rib, and collected it in a labeled container (ID number, age, sex, cause of death) for future processing. Although no minimum/maximum rib length was established, most samples obtained were between 3-7cm so that they could be accommodated by the gantry of the micro-Computed Tomography (micro-CT) imaging system.

SAMPLE PREPARATION

Once all samples were collected, a sample size of n=20 was determined appropriate for this project. This would allow two samples from each sex to be analyzed from five age ranges (50-59, 60-69, 70-79, 80-89, 90-99+). However, there is one

exception - there was only one viable sample for a male aged 50-59. A female aged 101 was analyzed instead. The ribs were cleared of virtually all remaining soft tissue and periosteum, as not to cause interference during imaging. Each rib was removed from its labeled container and placed into a bath of warm water and Tergazyme; the solution was then incubated at 40^{o}C for approximately one hour to hasten the removal of unwanted tissue. Upon removal from the bath, a blunt instrument was used to scrap all soft tissue and periosteum off of the cortical surface. The medullary cavity was largely left intact, and some was removed only near the very distal ends of each rib. Upon completion of the soft tissue removal, each rib was returned to its own labeled container, submerged in 70% EtOH, and stored in a refrigerator. Costal samples were only removed from EtOH twenty-four hours ahead of scanning to ensure the bone was dry before proceeding.

SAMPLE IMAGING

A SkyScan 1172 desktop micro-CT system housed at the National Polymer Innovation Center at The University of Akron was used to image all rib samples. Care was taken to ensure the source was viable and the machine was in proper alignment at the start of each scan. Once alignment was confirmed, the sample was fixed to a brass mount compatible with the SkyScan set-up (**Figure 9**). Since any sample movement during scanning would be detrimental to image reconstruction/analysis, the ribs were adhered to the mount with dental wax and Parafilm. These are both radiolucent materials that easily withstood the moderately warm environment of the Micro-CT (~28^{o}C). Additionally, the wax and Parafilm helped to mount the sample vertically,

meaning that the cross section taken would be near-perpendicular to the orientation of the bone. This would aide in better image reconstruction/analysis later.

Each set of images for each sample was obtained by X-rays emanating from the SkyScan. An energy of 100keV was used (maximum for this equipment) for all samples. Before image acquisition, a ubiquitous set of parameters were set: 5.5um pixel size, bright & dark acquisition, Aluminum filter (0.5mm), and medium camera pixels (2000 x 1666). The vertical position of each sample varied, as this was adjusted depending on the size and shape of the bone. All images were obtained with a vertical position ranging between 27-36mm. This setting would not affect the quality of the images obtained, only the position at which the sample was scanned. Before initiating each scan, a rotation step of 0.20 was assigned, along with a frame averaging of 5. The camera was also 'offset' so that a double-wide image would be obtained. This ensured that the entire bone would be included in image acquisition, regardless of the width of the rib. Each scan required about four hours to complete, resulting in a collection of roughly 1,070 image files per sample. One such image can be seen in **Figure 10**.

SOFTWARE

Once the scan was complete, the data sets were transferred from an external hard drive to the Andronowski Lab computer for image processing. Image reconstruction was performed with NRecon (Bruker, Kortich, Belgium), a commercial GPU accelerated filtered back projection-based reconstruction software package. A protocol was created and used as a template for all data sets. It is important to note the

thresholds that were applied to each sample. The lower grey threshold was 94, and the upper was 255. These were applied to each dataset before reconstruction and before manually adjusting any settings. A rough cross-section can be seen in **Figure 11,** highlighting the importance of manual adjustment. Once reconstructed, CTAnalyser v. 1.15.4.0 (Bruker, Kontich, Belgium) was used to extract quantitative data from the reconstructed images using Individual Object Analysis. A protocol was used for the ribs, similar to what was done with NRecon during reconstruction. However, due to slight variation in each scan, manual adjustment of each sample was needed to ensure the highest quality. A finished cross-section, ready to be analyzed, can be seen in **Figure 12**. In the settings, 'Smoothing' was consistently applied between settings 1 and 3. The 'Misalignment' setting was altered more frequently, usually different for each sample to collect the most accurate data possible. Samples were previewed beforehand, to confirm that cortical pores were visible and represented well by the current settings. To reduce the time needed to collect data from each sample, a rectangular Region of Interest (ROI) was formed for each dataset to remove background pixels. An example of this can be seen in **Figure 13** where there is no ROI and **Figure 14** after the ROI was identified. This was done in CTAnalyser, where the 'dead space' surrounding the cross-section was removed, so that the program would not try to pull data from these regions. Although settings were adjusted for a cross-section at the center, the topmost and bottommost cut were also previewed to ensure the current settings were adequate and best represented the entire sample. Once it was determined the cross-sections was an accurate representation, each sample's image file was placed into CTAnalyser. This software would pull the necessary data: tissue volume (TV), canal volume (Ca.V), canal

surface area (Ca.S), cortical porosity (Ca.V/TV), canal surface to tissue volume (Ca.S/TV), canal diameter (Ca.Dm), canal separation (Ca.Sp), and number of objects (#).

STATISTICAL ANALYSIS

Given that the sample size for each age group (i.e - 60-69) was small, and only included a maximum of two samples from each sex for that age group, the normality of the dataset was a concern. To determine normality, probability plots for each parameter listed above were made. This was performed with a Ryan-Joiner (Shapiro-Wilk) test, and a *p*-value greater than 0.05 indicated a relatively normal set of data for that parameter. For three of the parameters: TV, Ca.V/TV, and Ca.S/TV, the *p*-values of the normality tests were below 0.05. In order to proceed with the statistical analysis, these data were first normalized. To do so, a Johnson transformation test was used for the TV, Ca.V/TV, and Ca.S/TV data. This resulted in probability plots with *p* -values greater than 0.05, and the data were modified accordingly. With the normality of the data supported (all Ryan-Joiner *p*-values >0.05, with most being >0.100), a 2-way ANOVA test could be conducted. The was the preferred method because it would allow the comparison of each of the eight quantitative parameters with respect to age, sex and the interaction between age and sex.

Results

All eight parameters were statistically analyzed with a two-way ANOVA, and their values for each parameter depicted on scatter plots. Note that all two-way ANOVA analyses were conducted to examine the difference in the parameter between sex and age with age acting as a covariant. The statistical output tables and scatterplots can both be found in **Appendix A**. Also located in **Appendix A** is a table of the means, standard deviation, and standard error for all the raw data, separated by sex.

TISSUE VOLUME

There was no reported statistical difference for TV for neither age, sex, nor an interaction between age and sex (p=0.768, 0.216 and 0.556 respectively). The mean TV for females was 4.24E+11 ± 2.69E+10 μm³, while the mean TV was 7.19E+11 ± 6.79E+10 μm³ for males. The values from the statistical test (two-way ANOVA) for TV can be found in **Table 1**, and the table of means from the raw data in **Table 9**. Note that the values for TV were normalized via a Johnson Transformation prior to statistical analysis. After transformation, a Shapiro-Wilk normality test showed a p-value of >0.100, supporting the normality of the data. **Figure 1** is a scatter plot that shows the relationship between TV with respect to age. This plot also differentiates normalized TV values for each sex, so that the difference between the two and how they change with age may be visualized. Neither sex shows a large change in TV as age increases, but males tend to have a higher TV than females at any given age.

CANAL VOLUME

For Ca.V, there was no reported statistical difference for age, with p= 0.598. There was a significant difference for Ca.V between sex (p=0.026). Furthermore, there was a significant difference in the interaction between age and sex (p=0.013). The mean Ca.V for females was 2.51E+08 ± 4.13E+07 µm³, while the mean Ca.V was 7.19E+11 ± 6.79E+10 µm³ for males. These values, along with others from the two-way ANOVA can be found in **Table 2**, and the table of means from the raw data in **Table 9**. Ca.V values did not need to be normalized, as a Shapiro-Wilk normality test showed a p-value of 0.770. **Figure 2** is a scatter plot that shows the relationship between Ca.V with respect to age. This plot also differentiates Ca.V values for each sex, so that the difference between the two and how they change with age can be observed. Females appear to show a decrease in Ca.V as age increases. Males showed a slight increase based on this plot, but an outlier may have skewed the best fit line.

CORTICAL POROSITY

Note that cortical porosity was calculated as a ratio of canal volume to tissue volume, hence the abbreviation: Ca.V/TV. We reported no statistical difference in Ca.V/TV for age, with p= 0.619. There was a significant difference for Ca.V/TV between sex (p=0.011). Furthermore, there was a significant difference in the interaction between age and sex (p=0.013). The mean Ca.V/TV for females was 6.19E-02 ± 1.23E-02%, while the mean Ca.V/TV was 5.18E-02 ± 1.02E-02% for males. The statistical output from the two-way ANOVA can be found in **Table 3**, and the table of means from the raw

data in **Table 9**. Note that the values for Ca.V/TV were normalized via a Johnson Transformation prior to statistical analysis. After transformation, a Shapiro-Wilk normality test showed a *p*-value of >0.100, supporting the normality of the data. **Figure 3** is a scatter plot that shows the relationship between Ca.V/TV with respect to age. This plot also shows normalized Ca.V/TV values for each sex. Sex appears to have an opposing effect on Ca.V/TV, as Ca.V/TV increased with age for males but decreased with age for females.

CANAL SURFACE

Canal Surface (Ca.S) can also be considered Bone Surface Area. There was no reported statistical difference for age (p=0.757) nor sex (p=0.077). However, there was a significant difference in the interaction between age and sex (p=0.044). The mean Ca.S for females was 4.11E+07 ± 7.12E+06 µm², while the mean Ca.S was 5.66E+07 ± 6.66E+06 µm² for males. These values, along with others from the two-way ANOVA can be found in **Table 4**, and the table of means from the raw data in **Table 9**. Ca.S values did not need to be normalized, as a Shapiro-Wilk normality test showed a *p*-value of 0.837. **Figure 4** is a scatter plot that shows the relationship between Ca.S with respect to age. This plot also differentiates Ca.S values for each sex, so that the difference between the two and how they change with age can be seen. Females appear to show a decrease in Ca.S as age increases. Males showed a slight increase in Ca.S with age in this figure.

CANAL SURFACE TO TISSUE VOLUME

For Ca.S/TV, there was no reported statistical difference for age (p=0.666). There was a significant difference between sex (p=0.033) and the interaction between age and sex (p=0.045). The mean Ca.S/TV for females was 1.60E-04 ± 6.07E-05 1/µm, while the mean Ca.S/TV was 8.83E-05 ± 1.77E-05 1/µm for males. The statistical output from the two-way ANOVA can be found in **Table 5**, and the table of means from the raw data in **Table 9**. Note that the values for Ca.S/TV were normalized via a Johnson Transformation. After transformation, a Shapiro-Wilk normality test showed a p-value of >0.100, supporting the normality of the data. **Figure 5** is a scatter plot that shows the relationship between Canal Surface to Tissue Volume (Ca.S/TV) with respect to age. This plot also differentiates normalized Ca.S/TV values for each sex. Females appear to show a decrease in Ca.S/TV as age increases. Males showed a slight increase in Ca.S/TV with age in this figure. However, it should be noted that a fair bit of variance is present among the data for both sexes.

CANAL DIAMETER

There was no reported statistical difference for neither age, sex, nor an interaction between age and sex (p=0.796, 0.684 and 0.924 respectively) for Ca.Dm. The mean Ca.S/TV for females was 25.6 ± 2.18 µm, while the mean Ca.S/TV was 31.1 ± 1.70 µm for males. The statistical output from the two-way ANOVA can be found in **Table 6**, and the table of means from the raw data in **Table 9**. Note that the values for Ca.Dm were normalized via a Johnson Transformation. After transformation, a Shapiro-

Wilk normality test showed a *p*-value of >0.100, supporting the normality of the data. **Figure 6** is scatter plot showing the relationship between the (Ca.Dm) and age. This plot also differentiates normalized Ca.Dm values for each sex. Neither males nor females appeared to show a dramatic change in Ca.Dm as age increases. There also appears to be a lot of variance within the sexes. The results of the ANOVA agree with the appearance of the data in the scatter plot.

CANAL SEPARATION

This parameter represents separation of trabeculae in each sample. We reported no statistical difference for Ca.Sp for neither age, sex, nor an interaction between age and sex (*p*=0.796, 0.398 and 0.363 respectively). The mean Ca.Sp for females was 2.02E+03 ± 1.67E+02 µm, while the mean Ca.Sp was 1.94E+03 ± 1.45E+02 µm for males. These values, along with others from the two-way ANOVA can be found in **Table 7**, and the table of means from the raw data in **Table 9**. These values did not need to be normalized, as a Shapiro-Wilk normality test showed a *p*-value of 0.594. **Figure 7.** is a scatter plot showing the relationship between Ca.Sp with respect to age This plot also differentiates Ca.Sp values for each sex, so that the difference between the two and how they change with age can be seen. There appears to be some slight change in Ca.Sp with age, but there is a lot of variance in the data within sex, and little difference between the sexes as shown by this plot. The similar data distribution seen in the plot is reflected by the statistical analysis.

NUMBER OF OBJECTS

The No. value for this study pertains to the number of canals present. For No., there was no reported statistical difference for neither age, sex, nor an interaction between age and sex (p=0.718, 0.614 and 0.484 respectively). The mean No. for females was 7.04E+03 ± 1.39E+03, while the mean No. was 9.52E+03 ± 1.99E+03 for males. The statistical output from the two-way ANOVA can be found in **Table 8**, and the table of means from the raw data in **Table 9**. Note that the values for No. were normalized via a Johnson Transformation. After transformation, a Shapiro-Wilk normality test showed a p-value of >0.100, supporting the normality of the data. **Figure 8.** is a scatter plot showing the relationship between the No. and age. This plot also differentiates normalized No. values for each sex. Neither sex showed a dramatic change in No. as age increased. There does not also appear to be a large difference between the sexes.

Discussion

This study highlighted several important points present in existing literature. It has been noted that rib demonstrates high rates of remodeling (Epker and Frost 1965), and there are studies that note higher rates of remodeling in women, especially postmenopausal women (Parfitt 1984, Seeman 2013). Given that the female samples ranged from 58-101 years of age, this study targets that subset of females well. This point can be underscored when examining the statistical differences noted during data analysis. For cortical porosity, a strong indicator of remodeling (Agnew and Stout 2012), we observed a *p*-value of 0.011. Females had a mean cortical porosity of 0.0619 ± 0.0123%, while males had 0.0518 ± 0.0102%. These values are represented by a measure of canal volume over tissue volume (Ca.V/TV). It is important to note that even though no significance was noted between sex and TV ($p = 0.216$), a significant difference was noted in Ca.V ($p = 0.026$). This again alludes to the existing studies showing higher remodeling rates greater net bone loss in females vs. males (Dominguez and Stout 2016, Bell et al. 2001, Seeman 2013).

For all four parameters reporting significant differences: Ca.V, Ca.V/TV, Ca.S and Ca.S/TV, all of them showed significance at the interaction between age and sex. This is represented by the Age*Sex notation on **Figures 2-5**. This is interesting, as none of them showed any significance within age of one sex, but this Age*Sex interaction may provide support for age effecting Ca.V, Ca.V/TV, Ca.S and Ca.S/TV of each sex differently. That is to say, age may have a larger impact on microstructure when also comparing the sexes, rather than observing differences among age within only males or females. Age-related changes to bone are well-documented, but may consider the

bone's properties on the macroscopic level such as force before fracture (Agnew et al. 2015) or make predictions based on the known mechanism of bone remodeling and how age effects them (Seeman 2013). Furthermore, many aged-related changes within a sex have been confirmed in only weight bearing bone, which is subject to a myriad of different forces and in greater magnitude compared to rib (Bell et al. 2001, Parfitt 1984).

For this study, support has been offered for significant differences in bone microarchitecture between the two sexes. However, further investigation must be completed to establish causality between age and bone microstructure. The analysis performed here may indicate a relationship between age and sex, begging additional studies to find if age is affecting each sex differently in a significant, quantitative way. A larger sample size is critical for anyone who wants to explore the differences in microstructure of non-weight bearing bone. For each age cohort, a maximum of 2 samples were used for each sex. Small sample sizes may cause issues when we report a TV of 5.58E+11um^3 for a 57-year-old male, but a 7.42E+11um^3 for a male almost four decades older, as an example. Without further quantitative support, it cannot be said if this is typical or very far from normal, and certainly no statements of causality may be made. All in all, we have provided support for the microstructural dichotomy between the sexes, but more work must be done to fully explain the effects of age on a non-weight bearing bone.

Conclusions

This study has allowed for a deeper look into the relationship between age, sex and bone microstructure. With this study, we provided statistical support for the quantitative differences in bone microarchitecture between the sexes. The significant differences noted in Ca.V, Ca.V/TV, Ca.S and Ca.S/TV offer several interesting points when compared with pre-existing literature. All four parameters listed above that reported significance did so with respect to sex, in that each parameter differed between sexes. These findings are currently well-documented, highlighting increased remodeling in post-menopausal women (Seeman 2013). However, no significant difference was noted among age within either sex. Existing studies offer conflicting support (Agnew et al. 2015, Parfitt 1984). Although, these studies did not present high-resolution quantitative data to the same degree or placed focused on weight bearing bone.

Given that ribs show higher remodeling rates compared to weight bearing bone (Epker and Frost 1965), this may suggest that age should show a difference in microstructure given that net bone loss due to remodeling tends to increase with age. Although the data from this study did not show significance among age within a sex, there were still significant differences noted in the interaction between age and sex. This significance may allude to the idea that age affects sex differently, and that may only become apparent when comparing age between the two sexes.

The biggest hinderance to this study was the small sample size for each age group. For any given age group (50-59, 60-69, etc.), the sample size was not larger than 2 for each sex. This made it difficult to determine the effects of age on bone microstructure within one sex quantitatively, as there is a large degree of variation in the

parameters we tested for (see **Table 9**). Fortunately, more support for age-related changes in bone microarchitecture may be provided in the future when a larger sample size is present.

Appendix A

Source	DF	F-value	*p*-value	R^2 (%)
Age	1	0.09	0.768	-
Sex	1	1.67	0.216	-
Age*Sex	1	0.36	0.556	-
Model Summary	-	-	-	55.55

Table 1. A table showing the output of the two-way ANOVA for Tissue Volume (TV). Depicted here is the degrees of freedom, the F-value, the *p*-value, and the R^2 value for the model summary.

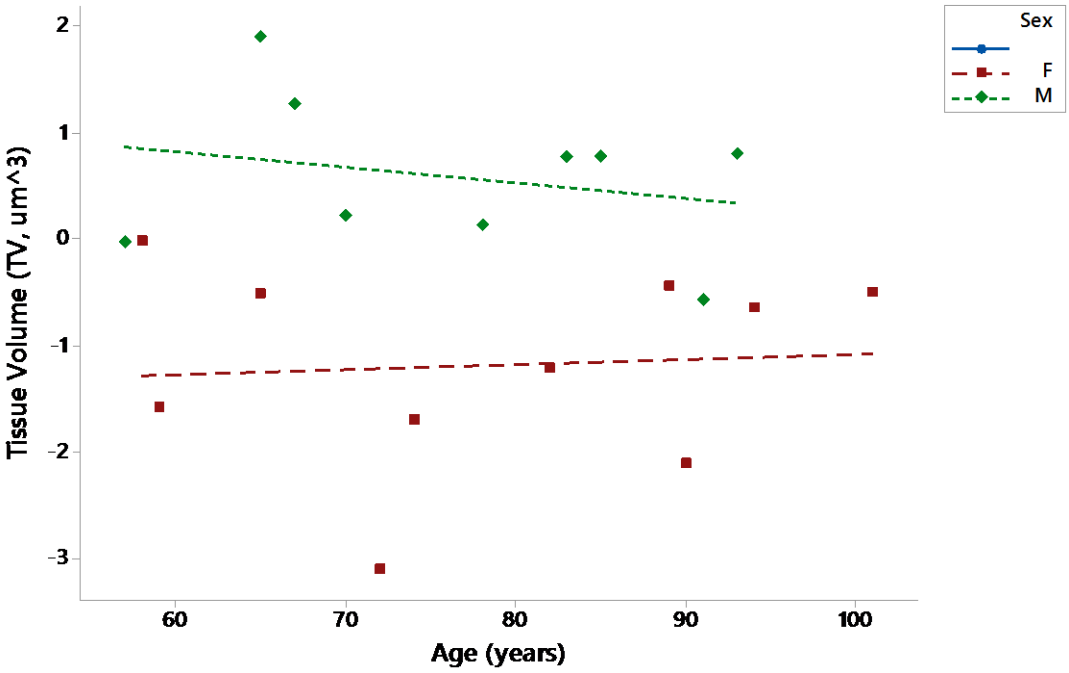

Figure 1. A scatter plot showing the relationship between the Tissue Volume (TV) and age. Also shown is the line of best fit for each sex.

Source	DF	F-value	*p*-value	R^2 (%)
Age	1	0.29	0.598	-
Sex	1	6.14	0.026	-
Age*Sex	1	7.85	0.013	-
Model Summary	-	-	-	46.08

Table 2. A table showing the output of the two-way ANOVA for Canal Volume (Ca.V). Depicted here is the degrees of freedom, the F-value, the *p*-value, and the R^2 value for the model summary.

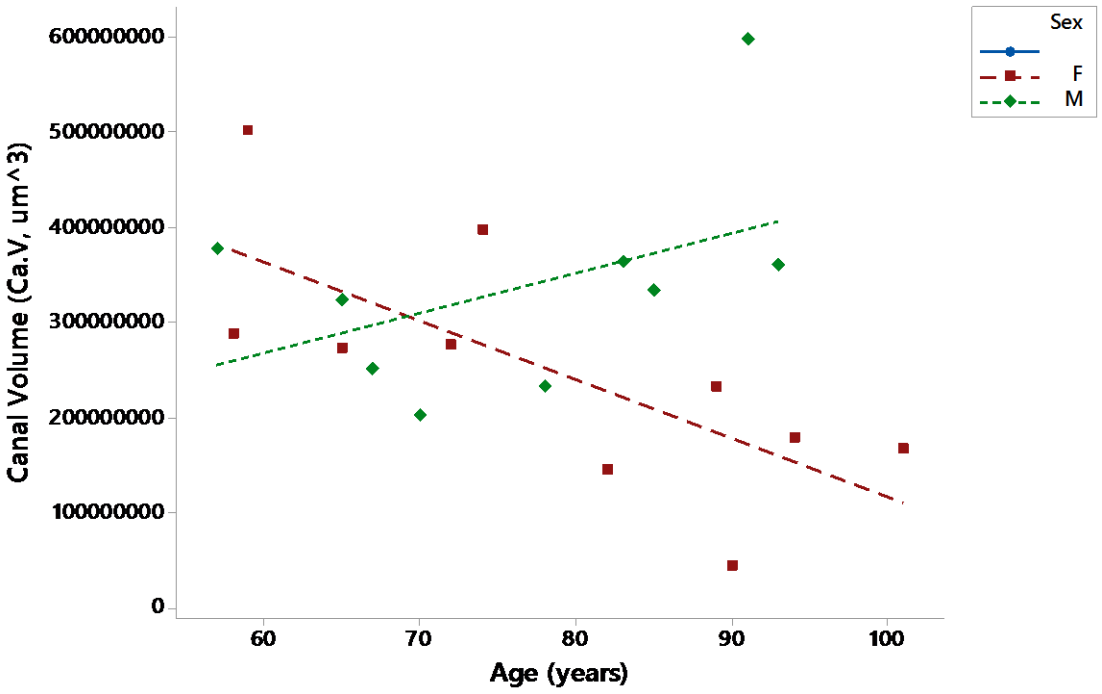

Figure 2. A scatter plot showing the relationship between the Canal Volume (Ca.V) and age. Also shown is the line of best fit for each sex.

Source	DF	F-value	*p*-value	R^2 (%)
Age	1	0.26	0.619	-
Sex	1	0.011	0.011	-
Age*Sex	1	7.94	0.013	-
Model Summary	-	-	-	39.66

Table 3. A table showing the output of the two-way ANOVA for Cortical Porosity (BV/TV). Depicted here is the degrees of freedom, the F-value, the *p*-value, and the R^2 value for the model summary.

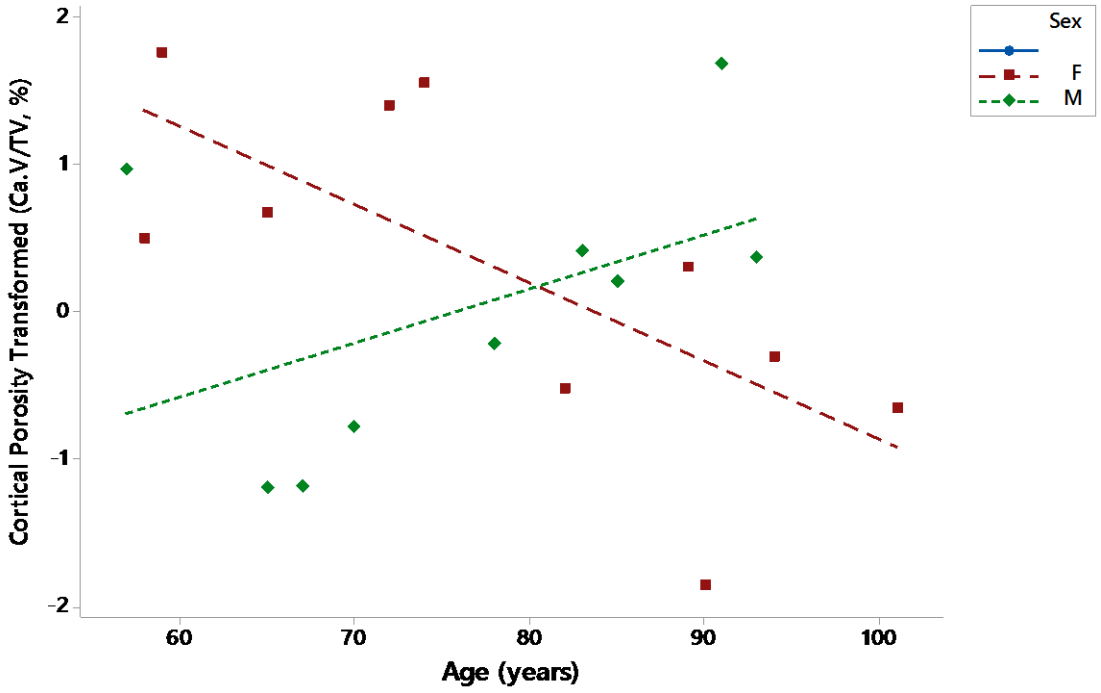

Figure 3. A scatter plot showing the relationship between the Cortical Porosity (BV/TV) and age. Also shown is the line of best fit for each sex.

Source	DF	F-value	*p*-value	R^2 (%)
Age	1	0.10	0.757	-
Sex	1	3.60	0.077	-
Age*Sex	1	4.85	0.044	-
Model Summary	-	-	-	36.56

Table 4. A table showing the output of the two-way ANOVA for Canal Surface (Ca.S). Depicted here is the degrees of freedom, the F-value, the *p*-value, and the R^2 value for the model summary.

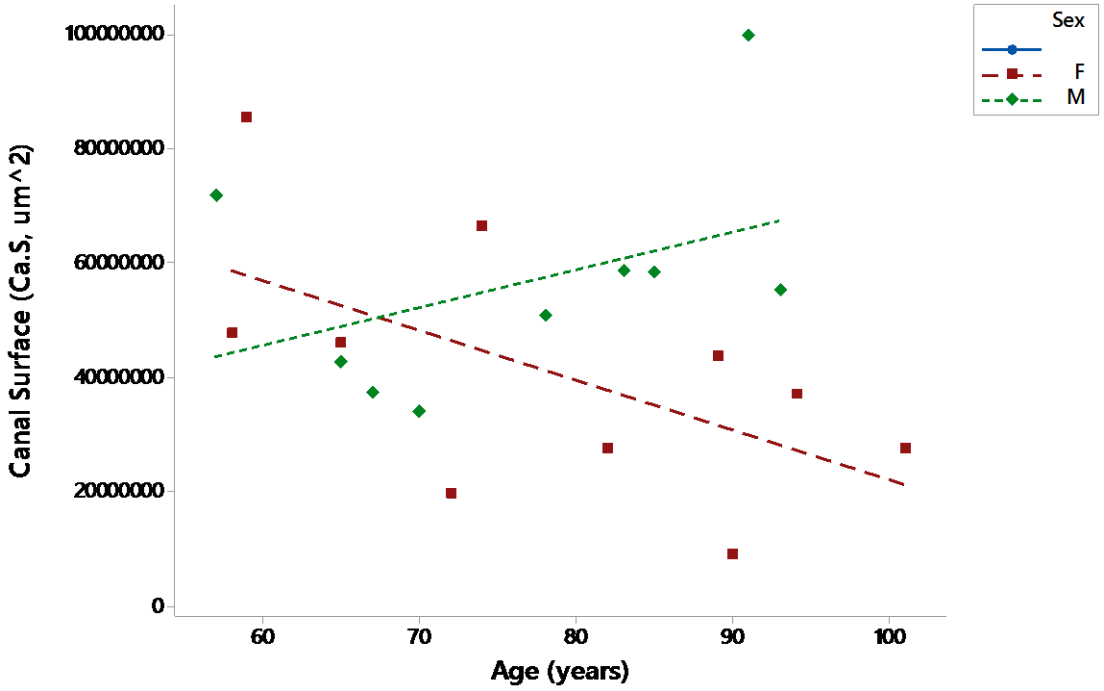

Figure 4. A scatter plot showing the relationship between the Canal Surface (Ca.S) and age. Also shown is the line of best fit for each sex.

Source	DF	F-value	*p*-value	R^2 (%)
Age	1	0.19	0.666	-
Sex	1	5.50	0.033	-
Age*Sex	1	4.78	0.045	-
Model Summary	-	-	-	31.76

Table 5. A table showing the output of the two-way ANOVA for the Canal Surface to Tissue Volume ratio(Ca.S/TV). Depicted here is the degrees of freedom, the F-value, the *p*-value, and the R^2 value for the model summary.

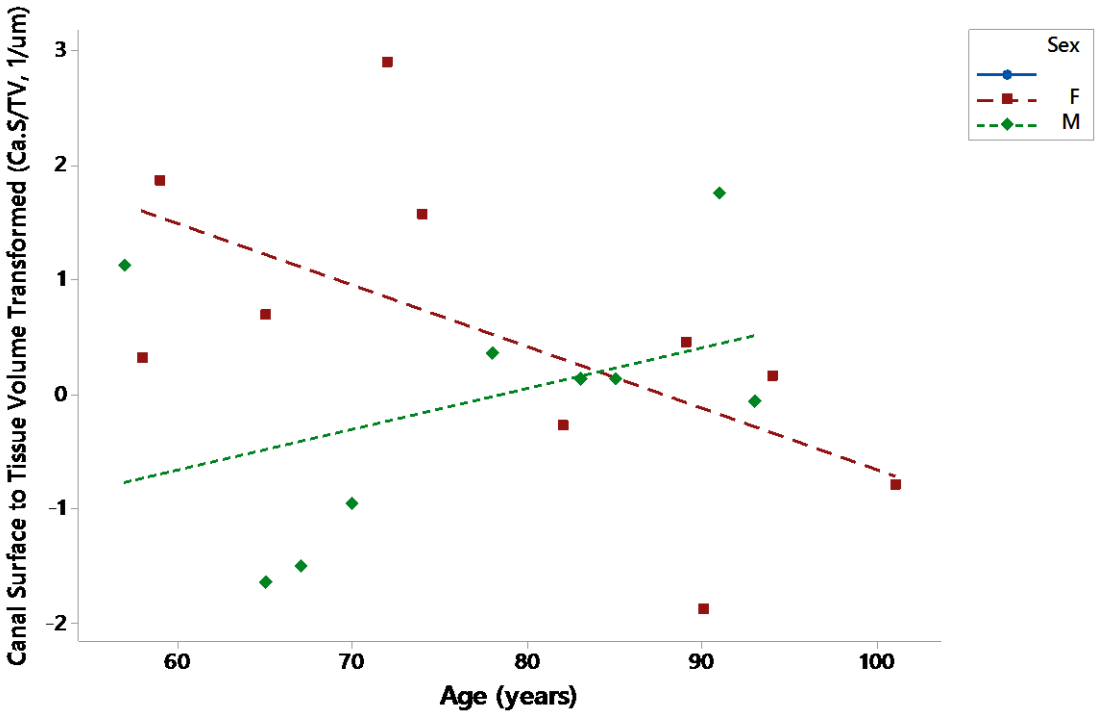

Figure 5. A scatter plot showing the relationship between the Canal Surface to Tissue Volume ratio (Ca.S/TV) and age. Also shown is the line of best fit for each sex.

Source	DF	F-value	*p*-value	R^2 (%)
Age	1	0.07	0.796	-
Sex	1	0.17	0.684	-
Age*Sex	1	0.01	0.924	-
Model Summary	-	-	-	20.39

Table 6. A table showing the output of the two-way ANOVA for Canal Diameter (Ca.Dm). Depicted here is the degrees of freedom, the F-value, the *p*-value, and the R^2 value for the model summary.

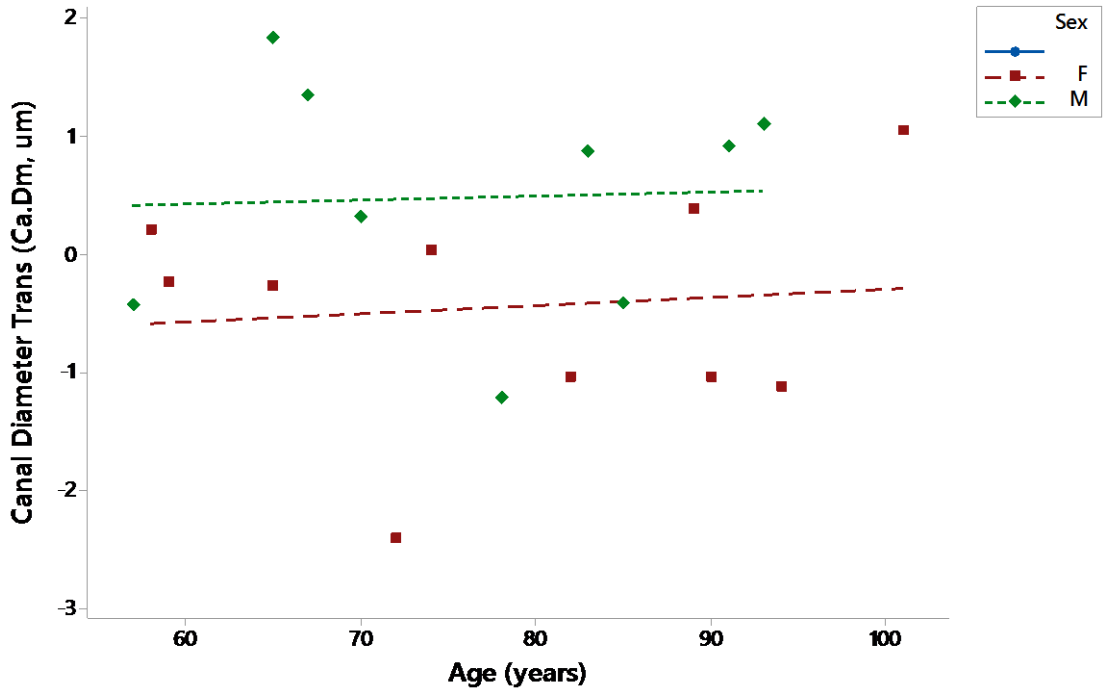

Figure 6. A scatter plot showing the relationship between the Canal Diameter (Ca.Dm) and age. Also shown is the line of best fit for each sex.

Source	DF	F-value	*p*-value	R^2 (%)
Age	1	0.07	0.796	-
Sex	1	0.76	0.398	-
Age*Sex	1	0.88	0.363	-
Model Summary	-	-	-	7.80

Table 7. A table showing the output of the two-way ANOVA for Canal Separation (Ca.Sp). Depicted here is the degrees of freedom, the F-value, the *p*-value, and the R^2 value for the model summary.

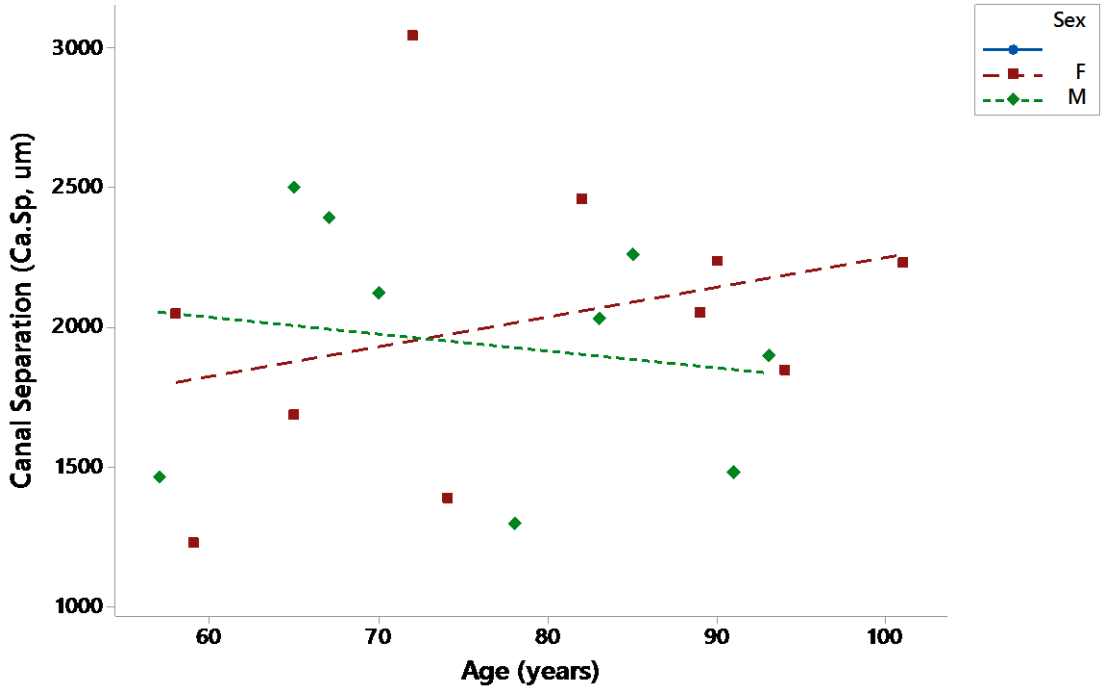

Figure 7. A scatter plot showing the relationship between the Canal Separation (Ca.Sp) and age. Also shown is the line of best fit for each sex.

Source	DF	F-value	*p*-value	R^2 (%)
Age	1	0.14	0.718	-
Sex	1	0.27	0.614	-
Age*Sex	1	0.51	0.484	-
Model Summary	-	-	-	11.31

Table 8. A table showing the output of the two-way ANOVA for the Number of Objects (#), which represents the number of canals. Depicted here is the degrees of freedom, the F-value, the *p*-value, and the R^2 value for the model summary.

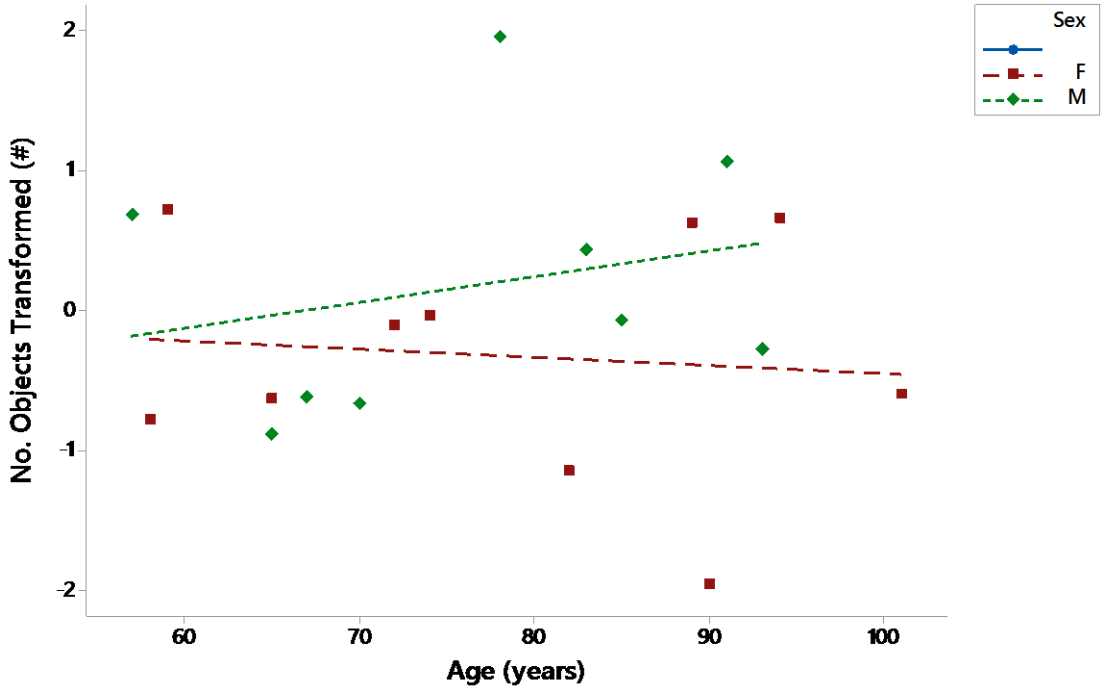

Figure 8. A scatter plot showing the relationship between the Number of Objects (#) and age. The Number of Objects represents the number of canals. Also shown is the line of best fit for each sex.

	TV (µm³)	Ca.V (µm³)	Ca.V/TV (%)	Ca.S (µm²)	Ca.S/TV (1/µm)	Tb.Th (µm)	Tb.Sp (µm)	No. of Objects (#)
Mean (F)	4.24E+11	2.51E+08	6.19E-02	4.11E+07	1.60E-04	2.56E+01	2.02E+03	7.04E+03
St. Dev (F)	8.51E+10	1.30E+08	3.88E-02	2.25E+07	1.92E-04	6.88E+00	5.29E+02	4.38E+03
SE (F)	2.69E+10	4.13E+07	1.23E-02	7.12E+06	6.07E-05	2.18E+00	1.67E+02	1.39E+03
Mean (M)	7.19E+11	3.38E+08	5.18E-02	5.66E+07	8.83E-05	3.11E+01	1.94E+03	9.52E+03
St. Dev (M)	2.04E+11	1.16E+08	3.05E-02	2.00E+07	5.31E-05	5.09E+00	4.35E+02	5.98E+03
SE (M)	6.79E+10	3.87E+07	1.02E-02	6.66E+06	1.77E-05	1.70E+00	1.45E+02	1.99E+03

Table 9. A table showing the mean, standard deviation (St. Dev) and standard error to the mean (SE) for each sex, for all eight quantitative parameters.

Appendix B

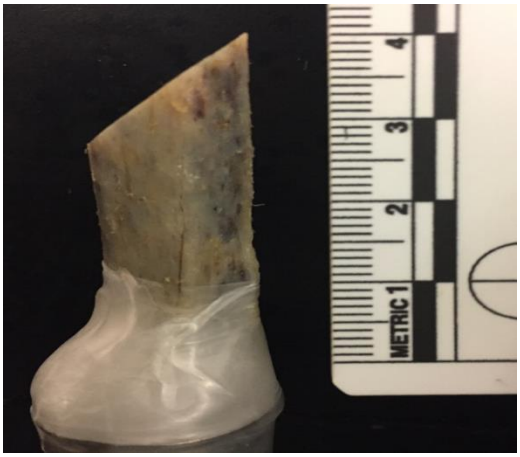

Figure 9. An image of a left sixth rib sample secured to a brass mount with dental wax and Parafilm before scanning in the SkyScan 1172 desktop X-ray system. Ruler on the side to indicate average sample length.

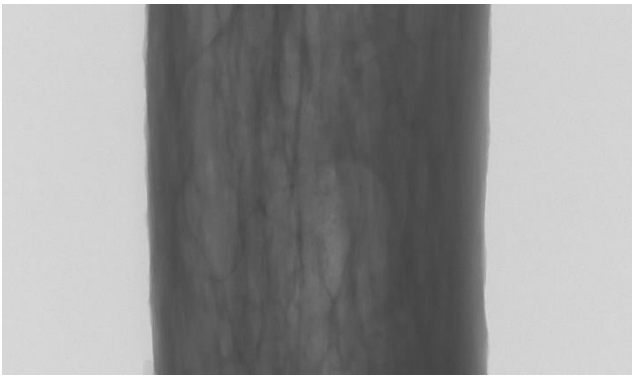

Figure 10. A rough 3D render of a rib from the Micro-CT before reconstruction through NRecon.

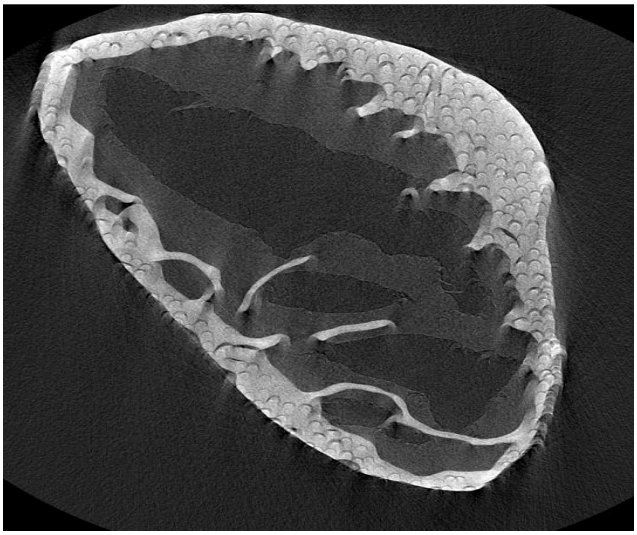

Figure 11. A cross-section of a rib sample in NRecon prior to manual adjustment. The cortical pores are nearly impossible to differentiate.

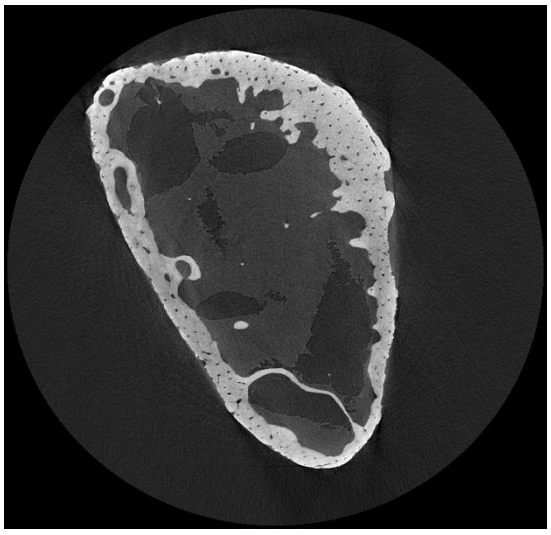

Figure 12. After manual adjustment, this NRecon cross-section shows cortical pores much more clearly, allowing proper quantitative analysis.

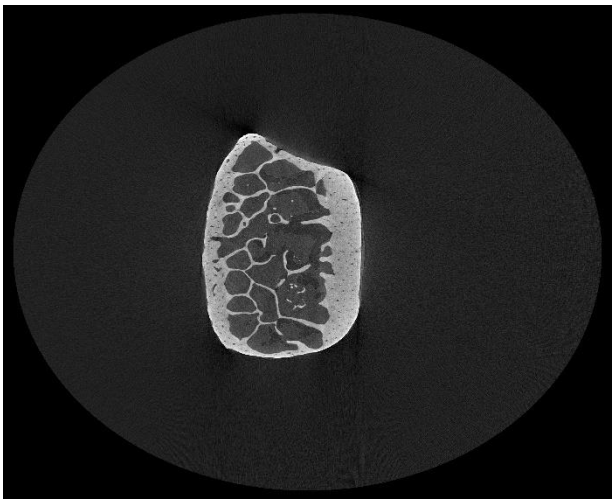

Figure 13. A cross-section of a rib sample in NRecon prior to quantitative analysis with CTAnalyser. Without a Region of Interest (ROI) specified, the program would try to take measurements on everything within the grey circle.

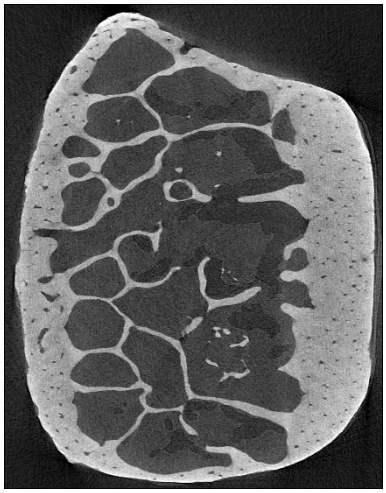

Figure 14. A cross-section of a rib sample in NRecon prior to analysis with CTAnalyser. With a ROI identified, CTAnalyser ran only within the bounds of the image above. This caused faster turnover time and credible quantitative data.

Acknowledgments

We thank the medical schools whose labs provided the samples for this study: Northeastern Ohio Medical University, The University of Toledo College of Medicine and Life Sciences, and Kent State University. Thanks to Dr. Andrew Knoll at the National Polymer Innovation Center for his instruction on how to properly operate the micro-CT instrument and his assistance during the sample scanning phase of the study. I also would personally like to give thanks to Dr. Janna Andronowski and Reed Davis for providing the outline for this project and guiding me along the way, as well as the Honors College at The University of Akron for this opportunity. Most of all, my thanks goes to the individuals who made such a noble sacrifice so that we may learn more from them.

References

Agnew, A.M., et al. “The Effect of Age on the Structural Properties of Human Ribs.” *Journal of the Mechanical Behavior of Biomedical Materials*, vol. 41, 2015, pp. 302–314.

Agnew, A.M., and S.D. Stout. “Brief Communication: Reevaluating Osteoporosis in Human Ribs: The Role of Intracortical Porosity.” *American Journal of Physical Anthropology*, vol. 148, no. 3, 2012, pp. 462–466.

Bell, K.L., et al. “Super-Osteons (Remodeling Clusters) in the Cortex of the Femoral Shaft: Influence of Age and Gender.” *The Anatomical Record*, vol. 264, no. 4, 2001, pp. 378–386.

Crowder C. 2005. Evaluating the use of quantitative bone histology to estimate adult age at death. Ph.D. Dissertation, University of Toronto, Department of Anthropology.

Dominguez, V.M., and A.M. Agnew. “Examination of Factors Potentially Influencing Osteon Size in the Human Rib.” *The Anatomical Record*, vol. 299, no. 3, 2016, pp. 313–324.

Epker, B.N., and H.M. Frost. “A Histological Study of Remodeling at the Periosteal, Haversian Canal, Cortical Endosteal, and Trabecular Endosteal Surfaces in Human Rib.” *The Anatomical Record*, vol. 152, no. 2, 1965, pp. 129–135.

Frost, H.M., “Tetracycline-Based Histological Analysis of Bone Remodeling.” *Calcified Tissue Research*, vol. 3, no. 1, 1969, pp. 211–237.

Hillewig, E., et al. “Magnetic Resonance Imaging of the Medial Extremity of the Clavicle in Forensic Bone Age Determination: A New Four-Minute Approach.” *European Society of Radiology*, no. 21, 3 Oct. 2010, pp. 757–767.

Karlson, K.A. “Rib Stress Fractures in Elite Rowers.” *The American Journal of Sports Medicine*, vol. 26, no. 4, 1998, pp. 516–519.

Kerley, E.R. “The Microscopic Determination of Age in Human Bone .” *American Journal of Physiological Anthropology*, no. 23, 1965, pp. 149–164.

Parfitt, A.M. “Age-Related Structural Changes in Trabecular and Cortical Bone: Cellular Mechanisms and Biomechanical Consequences.” *Calcified Tissue International*, vol. 36, no. S1, 1984.

Ritz-Timme, S., et al. “Age Estimation: The State of the Art in Relation to the Specific Demands of Forensic Practise.” *International Journal of Legal Medicine*, vol. 113, no. 3, 2000, pp. 129–136.

Seeman, E. “Age- and Menopause-Related Bone Loss Compromise Cortical and Trabecular Microstructure.” *The Journals of Gerontology Series A: Biological Sciences and Medical Sciences*, vol. 68, no. 10, 2013, pp. 1218–1225.

Taylor, A. “The Contribution of the Intercostal Muscles to the Effort of Respiration in Man.” *The Journal of Physiology*, vol. 151, no. 2, 1960, pp. 390–402.

Tommerup, L.J., et al. “Does Weight-Bearing Exercise Affect Non-Weight-Bearing Bone?” *Journal of Bone and Mineral Research*, vol. 8, no. 9, 2009, pp. 1053–1058.